Analyst

PAPER

View Article Online
View Journal | View Issue

Cite this: *Analyst*, 2026, **151**, 577

Elucidating time-resolved intracellular metabolic dynamics *via* label-free Raman microspectroscopy and 2D correlation spectroscopy

Zohreh Mirveis, *[a,b] Nitin Patil [a,b] and Hugh J. Byrne [a]

Understanding dynamic metabolic processes is central to elucidating cellular function and disease mechanisms. Glycolysis and glutaminolysis are particularly important, as they support bioenergetic and biosynthetic pathways, and their dysregulation is strongly linked to disorders. Raman spectroscopy provides a powerful, non-invasive approach for probing cellular dynamics, and recent advances in instrumentation and computational analysis have enhanced its sensitivity, enabling detection of subtle metabolic variations in complex environments. In this study, Raman spectroscopy combined with two-dimensional correlation spectroscopy (2D-COS) was applied to investigate metabolic responses of cells exposed either to glucose alone or glucose supplemented with glutamine, with emphasis on glutamine's effect on overall metabolic dynamics. Cells were starved for 2 h and then exposed to nutrients, after which they were fixed at 15 minute intervals for up to 2 h and spectroscopically monitored to evaluate the kinetic evolution of the metabolic response. To validate the approach, simulated datasets were initially used to model simplified metabolic pathway dynamics, which confirmed that 2D-COS could reliably track the kinetic evolution of simulated variables, even in the presence of high background interference. Analysis of cellular spectra revealed systematic temporal changes across biomolecular bands, suggesting partial synchronisation of metabolic responses, with oscillatory patterns observed under glucose-only conditions. In contrast, glucose–glutamine samples showed accelerated and amplified metabolic variability, with stronger correlations and additional variable bands, particularly linked to nucleic acid vibrations. Overall, these findings demonstrate the utility of Raman 2D-COS for resolving intracellular metabolic dynamics from complex datasets, offering new opportunities for advancing diagnostics and therapeutic interventions.

Received 21st October 2025,
Accepted 5th December 2025

DOI: 10.1039/d5an01114k

rsc.li/analyst

1. Introduction

Understanding dynamic metabolic processes at the cellular level is fundamental to elucidating cellular functions and disease mechanisms.[1,2] Among these, the glycolysis and glutaminolysis pathways are of particular importance, as they provide not only energy but also biosynthetic precursors essential for cell growth and survival.[3,4] Dysregulation of these pathways has been closely associated with various disorders, including cancer, immune dysfunction, and neurological disorders.[5,6] As such, monitoring their kinetics offers valuable opportunities for developing diagnostic biomarkers and guiding therapeutic strategies.

Raman spectroscopy has emerged as a powerful, non-invasive tool for monitoring cellular metabolic dynamics, providing molecularly specific information without the need for labels or dyes.[7] In recent years, Raman-based strategies for metabolite detection have gained considerable attention, as highlighted in recent reviews.[8,9] Nevertheless, its full potential for molecular characterisation remains underexploited. A major limitation is that advances in data analysis and spectral mining have not kept pace with improvements in measurement technologies, thereby constraining the interpretation of complex cellular spectra.[10,11] In particular, analysis of time-resolved spectral datasets at the single-cell level is inherently challenging, as it requires extracting subtle variations from signals dominated by high cellular background contributions, and associated intrinsic variance.[12]

Two-dimensional correlation spectroscopy (2D-COS), introduced in 1989, provides a powerful framework for resolving subtle spectral variations induced by external perturbations such as time.[13] The utility of this technique for analysing complex cellular datasets has been demonstrated in multiple studies.[14–16] For instance, Lasch and Noda applied 2D-COS to spatially resolved hyperspectral images (HSI), demonstrating

[a]*FOCAS Research Institute, TU Dublin, City Campus, Camden Row, Dublin 8, Ireland. E-mail: D21127294@mytudublin.ie*
[b]*School of Physics, Optometric and Clinical Sciences, TU Dublin, City Campus, Grangegorman, Dublin 7, Ireland*

its value for spectral band assignment and for detecting subtle correlations within and across imaging modalities.[17] Also, Wang *et al.* demonstrated the power of combining 2D-COS with deep learning for metabolomics, enhancing spectral resolution and facilitating classification in traceability analysis.[18] Another study by Byrne *et al.* validated the application of 2D-COS to time-resolved Raman datasets.[19] Their work combined simulated and experimental Raman data from doxorubicin-treated human lung cancer cells and demonstrated that 2D-COS can resolve different stages of the cellular response. In this study, synchronous correlation captured the immediate drug-binding events as well as longer-term metabolic changes, while asynchronous spectra enabled these processes to be separated and temporally resolved.

In this study, the potential of Raman spectroscopy combined with 2D-COS was investigated to track metabolic dynamics in cells exposed to either glucose alone or a glucose–glutamine mixture, under conditions established in previous studies.[3,20] This approach enabled the assessment of cellular responses to nutrient availability, with particular emphasis on the effect of glutamine supplementation on overall metabolic behaviour. 2D-COS was applied to resolve these metabolic changes and to compare the intracellular responses between the two nutritional conditions. As the aim of this work was to capture systematic and simultaneous changes in intracellular metabolism, the synchronous 2D-COS map, highlighting coordinated, in-phase intensity variations, was considered the most relevant and was therefore employed. As sequential or time-delayed processes were not the focus of this study, the asynchronous map was not required.

To explore the data-mining potential of 2D-COS, simulated datasets representing simplified metabolic pathway dynamics were first used to evaluate the method under conditions of overlapping signals and strong cellular background. Two ODE-based kinetic models, sequential (A → B → C) and parallel (A → C and B → C), were constructed to represent glycolysis and the interplay between glycolysis and glutaminolysis, respectively. These models were based on a previously developed glycolysis–glutaminolysis model but were simplified further here to serve as a proof-of-principle framework, enabling the reproduction of simplified consumption-formation kinetics for evaluating the 2D-COS analysis method.[3] The resulting kinetic profiles were then superimposed as perturbations onto cellular spectra to (1) introduce intercellular variability by incorporating 25 different single-cell spectra at each time point, and (2) to assess the detectability of subtle kinetic changes by progressively increasing the contribution of the cellular background. This incorporation of real cellular data was designed to mimic known intracellular data-mining challenges and to generate realistic yet simplified representative conditions for assessing the performance of 2D-COS. Data analysis was performed using synchronous maps generated through auto-correlation of the spectral dataset. In auto-correlation 2D-COS, a dataset is correlated with itself to capture the internal consistency of spectral variations. The resulting synchronous maps display diagonal peaks that reflect the magnitude of temporal intensity changes, and monitoring their evolution enabled the extraction of underlying metabolic dynamics. The subsequent analysis of cellular data with this technique reliably revealed distinct dynamical variations under both nutritional conditions and highlighted the role of glutamine in accelerating metabolic dynamics, amplifying overall variability, and contributing to biosynthetic processes.

Overall, this study demonstrates the analytical potential of 2D-COS for time-resolved single-cell Raman spectroscopy through the evaluation of cellular responses under different nutritional conditions. By identifying subtle correlations in the evolution of spectral features and revealing coordinated molecular variations that are often obscured by high cellular background, 2D-COS provides a powerful framework for detecting early metabolic shifts and enhancing the interpretability of intracellular dynamics. These capabilities position 2D-COS as a promising tool for high-content drug screening, metabolic phenotyping, and the development of Raman-based diagnostic markers of cellular dysfunction.

2. Methodology

2.1. Cell culture & seeding

Monkey kidney (LLC-MK2) cells were cultured in DMEM (Sigma Aldrich, Ireland) supplemented with 10% FBS (MSC-qualified; Sigma Aldrich, Ireland) and 1% penicillin–streptomycin (GIBCO, ThermoFisher, Ireland) at 37 °C in a humidified 5% CO_2 incubator. Cells were seeded at 71.1×10^4 cells per well on top of the glass already placed in 12 well plate. The reason the glass placed at the bottom of each well plate, is that the polystyrene has many sharp peaks and most of them overlap on cellular key peaks like phenylalanine. Following the protocols established in previous studies,[3,4,21] and adapted from those of the commercially available glycolysis assay,[22] cells were starved prior to sample exposure. After seeding, they were incubated for 16 h in nutrient-rich medium, followed by a 2 h starvation period during which the medium was replaced with respiration buffer (RB) and the plates were placed in a CO_2-free incubator to deplete dissolved CO_2 and force the cells to consume their carbon reserves.

2.2. Sample exposure

After starvation, cells were exposed to two different nutritional conditions: (1) glucose alone (7.5 mM) and (2) a mixture of glucose (7.5 mM) and glutamine (2 mM). Then, cells were fixed at 15 min intervals for up to 2 h. Fixation was carried out by incubating the cells in 10% formalin for 15 min, followed by replacing the formalin with PBS to prevent over-fixation. This procedure ensured preservation of cellular morphology and proteins for subsequent analysis.

2.3. Raman setup and measurement

Fixed-cell Raman measurements were performed using a Horiba Jobin Yvon LabRAM HR system coupled to an upright Olympus BX41 microscope. A 532 nm laser served as the

source, and spectra were collected with a 100× water immersion objective (LUMPlanFL, ×100, Olympus) to enhance focus and light collection. Spectra were recorded over the 600–1800 cm^{-1} range, covering the so-called vibrational fingerprint region. At each time point, spectra were acquired from 25 individual cells, targeting the cytoplasmic region. Pure component spectra (glucose, glutamine, RNA, and lactate) used in the simulation datasets were acquired with the same setup, except with a 60× objective.

2.4. Data analysis

Data preprocessing. Following cellular spectral acquisition, raw spectra were pre-processed by first applying a Savitzky–Golay filter (polynomial order 5, frame length 9) to reduce high-frequency noise, followed by the adapted Extended Multivariate Signal Correction (EMSC) for background subtraction (glass + water), as described by Hennelly *et al.*[23] The polynomial order for EMSC was optimised by PCA clustering, order 5 being identified as the optimum. Further details are provided in SI.

2D-COS analysis. 2D-COS enhances spectral resolution by correlating intensity variations as a result, and as a function of an external perturbation, producing synchronous and asynchronous maps that describe simultaneous and sequential spectral changes, respectively.[24,25] In this study, the background-corrected data were analysed using 2D-COS to resolve coordinated metabolic variations under different nutritional conditions as a function of time. The computations were performed using the mat2dcorr MATLAB application,[26] with the spectral data formatted into the required structure, including the spectral matrix (spc), wavenumber vector (wav), and time variable (war). For the analysis, auto-correlation was carried out by loading the same dataset as both the X and Y inputs. Only synchronous maps were generated, as the focus of this study was on simultaneous, in-phase metabolic variations rather than asynchronous, sequential processes. The synchronous spectra were computed using the average spectrum as the internal reference, with the analysis restricted to the spectral region of 601–1800 cm^{-1}, as defined by the acquired Raman spectra. In the generated synchronous maps, yellow regions indicate positive correlations (bands varying in the same direction), while blue regions indicate negative correlations (bands varying in opposite directions). Diagonal autopeaks ($\nu_1 = \nu_2$) are always positive, with their amplitude reflecting the degree of temporal variation. In this study, peaks of the diagonal were used to identify the most variable spectral features, which were subsequently tracked in the spectra data to monitor their absolute changes over time.

2.5. Spectral simulations for evaluating 2D-COS

To establish a reference for cellular data analysis and to assess the ability of 2D-COS to detect the most variable bands under high background variance, simulated spectral datasets were generated. These datasets provided simplified representations of the pathways of interest, glycolysis and glutaminolysis. For glycolysis, a sequential metabolic model with three components (glucose → RNA → lactate) was constructed. RNA was chosen purely as a representative spectral component available in-house, and no physiological significance is implied by this label. The kinetic evolution of their concentrations was simulated using ordinary differential equations (ODEs) under a sequential scheme (A → B → C) with rate constants k_1 = 0.075 min^{-1} and k_2 = 0.02 min^{-1}. To represent the interplay between glycolysis and glutaminolysis, a parallel pathway model (A → C, B → C) was designed, using the same rate constants. In this model, both glucose and glutamine converge to the same end product, lactate, consistent with their established metabolic interactions.[27,28] Notably, the kinetic rate constants were selected to produce smooth, distinguishable temporal profiles and were not intended to represent physiologically measured reaction rates. Their specific values were informed in part by the study by Mirveis *et al.*, in which a glycolysis–glutaminolysis kinetic model was developed and trained using a kinetic assay.[3]

To evaluate whether temporal patterns of the main variables could still be detected under increasing cellular background noise, simulated data were constructed by superimposing the component variations onto the spectra of real cellular measurements, using the same 25 individual cell spectra at each time point. Spectra were acquired from human lung adenocarcinoma (A549) cells using a 785 nm laser (LabRam HR800, Horiba) over 600–1800 cm^{-1} with a ~1 μm spot size. The relative contribution of the cellular background was systematically increased, reducing the relative intensity of the variable signals and thereby evaluating the detection sensitivity of 2D-COS.

3. Results and discussion

3.1. Simulated data as a guide for evaluating and data mining in 2D-COS

The metabolic pathway was modelled as a progression of cellular states (A → B → C), each characterised by distinct spectral profiles. Each simulated component represents a spectral fluxome or fluxotype, an aggregate of overlapping vibrational signatures from multiple intracellular species.[29] The purpose of simulating intracellular dynamics was to evaluate whether 2D-COS could detect temporal transitions between these states and to provide an interpretable framework before applying the method to cellular measurements.

The simulated spectroscopic representation of the glycolysis pathway is shown in Fig. 1, providing a reference framework for interpreting the 2D-COS results. Fig. 1a presents the concentration profiles of glucose, RNA, and lactate over time, while Fig. 1b shows their spectral signatures, with characteristic peaks highlighted: glucose (1000–1200 cm^{-1}), RNA (~790 cm^{-1}), and lactate (~850 cm^{-1}). Fig. 1c presents the simulated dynamic profiles of the components, highlighting their continuous spectral intensity changes throughout the time course. Fig. 1d shows the temporal variation of these components superimposed on a cellular background (weight-

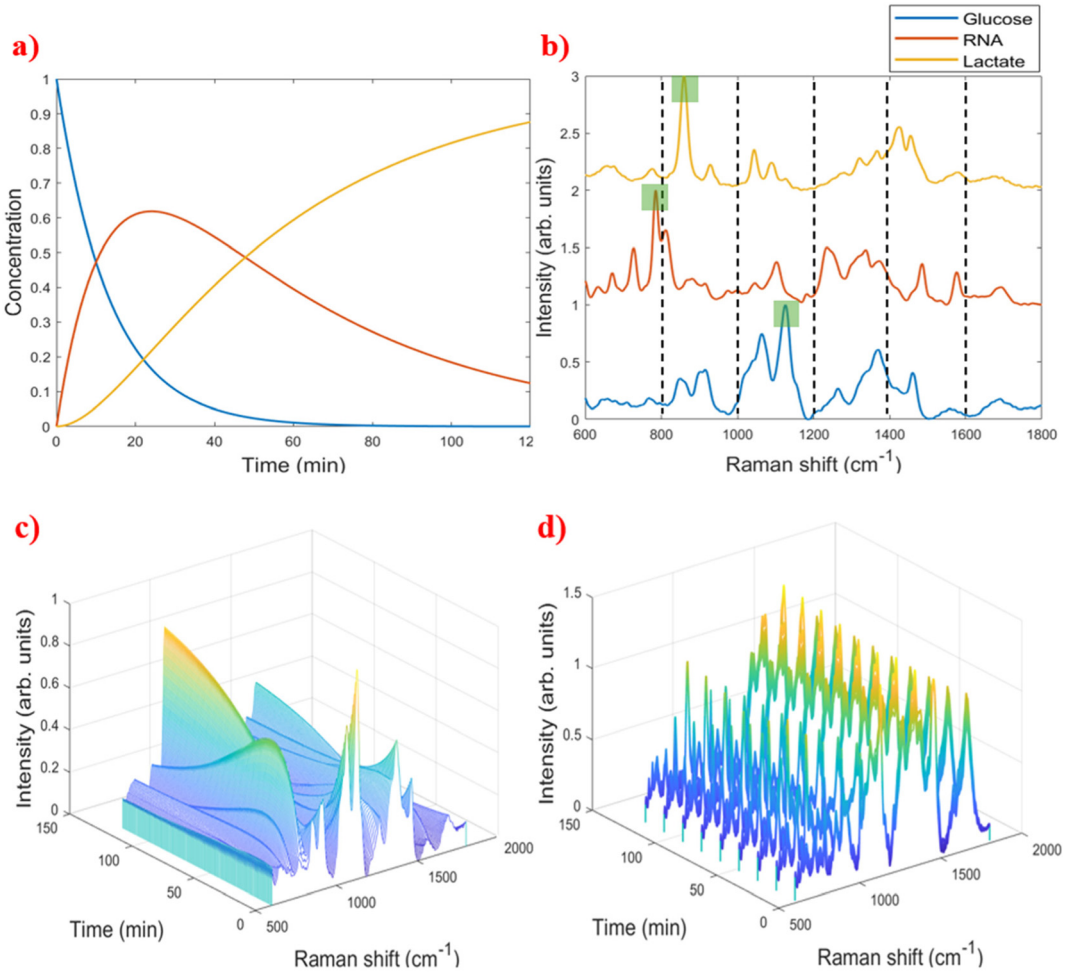

Fig. 1 Simulated representation of the glycolysis pathway. (a) Concentration profiles of glucose, RNA, and lactate over time. (b) Corresponding Raman spectral signatures with characteristic peaks highlighted. (c) Simulated time evolution of the spectral components over 2 h. (d) Temporal variation of the components combined with cellular spectra (25 cells per time point), discretised into 15 minute intervals.

ing = 1), generated from 25 cell spectra per time point and discretised into 15 minute intervals to mimic the experimental sampling conditions.

The simulated data analysed using 2D-COS, and the corresponding results are shown in Fig. 2. In the results, the synchronous map (Fig. 2a) shows a clear separation between positive (yellow) and negative (blue) correlations. As shown in Fig. 2b, vertical and horizontal slices at, for example ~1127 cm^{-1} and ~855 cm^{-1} do not return the pure spectra of any of the individual components, although they do indicate relative correlations between the different components, for example a negative correlation between lactate and glucose, one increasing as the other decreases, although the map alone does not specify direction. The slices also reveal further correlations; for example, the 1127 cm^{-1} band correlates positively with ~1380 cm^{-1}, suggesting either the same metabolite or distinct metabolites varying together.

The diagonal plot (Fig. 2c) reveals the peaks which vary systematically as a function of time, wherein higher intensities reflect stronger temporal variations. Characteristic bands of all three components clearly contribute, the strongest peaks appearing at 1125 cm^{-1} (glucose), 860 cm^{-1} (lactate), and 787 cm^{-1} (RNA). To track the temporal evolution of the diagonal peaks, all identified peaks were plotted with 25 replicates at each time point and subsequently averaged across time points to better visualise overall patterns (Fig. S3). Since several peaks showed nearly identical trends, one representative band was chosen for each variable to avoid redundancy, while preserving distinct spectral changes. As shown in Fig. 2d, the temporal evolution of the three identified characteristic peaks is clearly resolved and is consistent with the simulated data.

The results of increasing the cellular background to test the sensitivity of 2D-COS are shown in Fig. 3. In all cases, the average spectra were removed prior to 2D-COS analysis to ensure that only dynamic spectral variations contributed to the correlations. The results show that while component intensities decrease proportionally with increasing cellular weight, the temporal evolution patterns remain consistent up to a weighting of 40. The synchronous maps and diagonal peaks

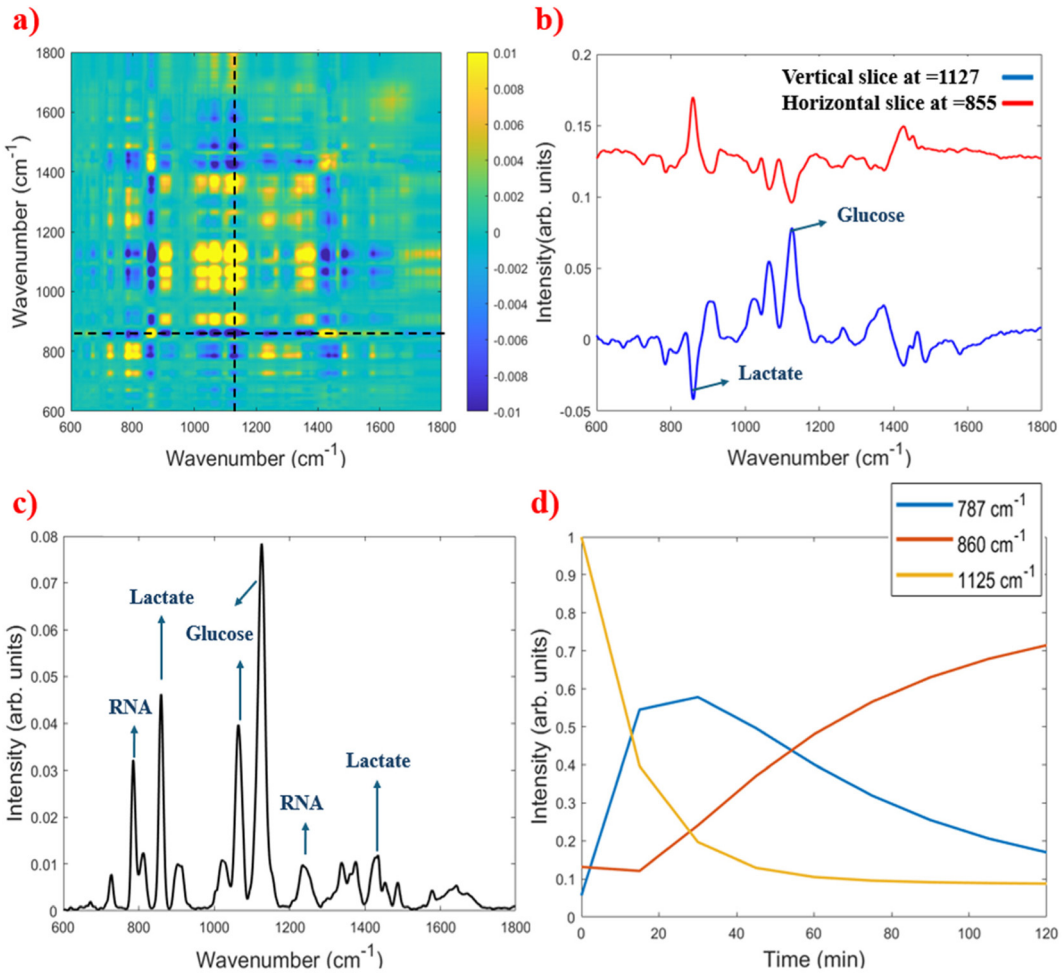

Fig. 2 2D correlation spectroscopy (2D-COS) results for simulated glycolysis pathway. (a) Auto-synchronous 2D-COS map. (b) Vertical and horizontal slices at 1127 and 855 cm^{-1}. (c) Diagonal of the 2D-COS map identifying the strongest variable peaks. (d) Temporal evolution of representative bands (787, 860, and 1125 cm^{-1}), consistent with simulated kinetics.

remain stable from weights 10 to 40, only the relative intensities changing (Fig. S4). This suggests that 2D-COS captures cellular background signals alongside the main variables; for example, strong peaks at 1000, 1337, and 1650 cm^{-1}, although their temporal evolution does not change significantly compared with the main variables (Fig. S5). Importantly, the key variables remain detectable even at a cellular weight of 40, underscoring the sensitivity and reliability of 2D-COS in extracting meaningful trends under strong cellular noise.

In the simulated model of the interplay of the glycolysis–glutaminolysis pathways (A → C, B → C), the main challenge arises from the overlap of two key variables, glucose and glutamine, both of which decrease over time but, with different dynamics. Despite this complication, the main variable peaks at 855 cm^{-1} (lactate), 1132 cm^{-1} (glucose), and 1333 cm^{-1} (glutamine) are well resolved in the auto-synchronous map (diagonal peaks), and their temporal evolution can be reliably tracked (results shown in Fig. S6). These kinetic trends are consistent with the simulated data, highlighting the effectiveness of the 2D-COS technique. Notably, the strongest glutamine peak near 850 cm^{-1} is completely overlapped by the lactate band at the same wavenumber, obscuring the glutamine trend in this region. However, the distinct glutamine peak at 1333 cm^{-1} serves as a reliable marker, accurately representing its kinetic behaviour.

3.2. Data mining of label-free spectral profiles of intracellular metabolism under two nutritional conditions

In comparison to the simulated datasets, the cellular data are inherently more complex, as countless biomolecular processes, including those related to growth, stress responses, and other cellular functions, fluctuate continuously alongside metabolic pathways.[30,31] Consequently, it is unrealistic to expect complete resolution of dynamic changes attributable to a single pathway such as glycolysis. What can be achieved, however, is a broad overview of the most variable features identified by the auto-synchronous map, which allows comparisons between the two nutritional conditions and provides insight into how glutamine supplementation influences the overall dynamic behaviour of the cells.

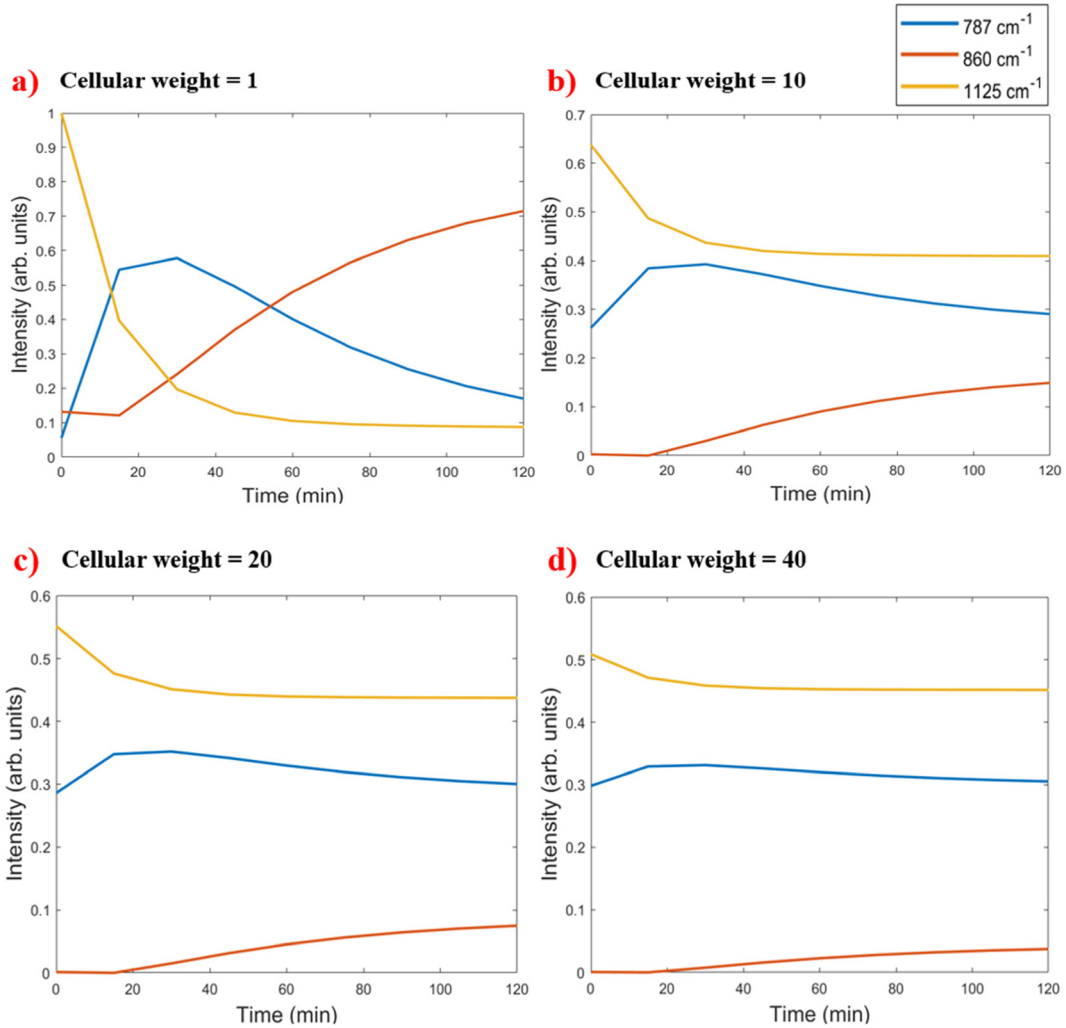

Fig. 3 Temporal evolution of representative peaks (787 cm^{-1}, RNA; 860 cm^{-1}, lactate; 1125 cm^{-1}, glucose) under increasing cellular background weights. (a) Weight = 1, (b) weight = 10, (c) weight = 20, and (d) weight = 40.

Spectral data obtained from LLC-MK2 cells exposed to two different nutritional conditions, (1) glucose alone and (2) a mixture of glucose and glutamine, were analysed using 2D-COS. The corresponding results are shown in Fig. 4, the left panels representing cells fed with glucose alone and the right panels representing cells fed with the glucose–glutamine mixture.

As shown in the auto-synchronous maps (Fig. 4a and b), both datasets display distinct regions of positive (yellow) and negative (blue) correlations. The correlation intensities are generally weaker for the glucose-only sample (scale bar: −0.08 to 0.08; Fig. 4a), whereas they are stronger for the glucose–glutamine sample (scale bar: −0.2 to 0.2; Fig. 4b), indicating greater spectral variability and enhanced dynamic behaviour when glutamine is added. In both conditions, the band around ~1440 cm^{-1} exhibits strong negative correlations with several other spectral regions, most notably with the band near ~780 cm^{-1}. This negative correlation is illustrated in the slice plots (Fig. 4c and d), whereby the vertical slices at ~780 cm^{-1} (red curves) and the horizontal slices at ~1440 cm^{-1} (blue curves) show clear opposing trends.

The diagonal plots provide further insight into the most variable peaks over time. In the glucose-only condition (Fig. 4e), among the pronounced peaks, the sharpest and most intense include those at ~1000 cm^{-1} (assigned to phenylalanine in proteins), ~1440 cm^{-1} (CH_2 vibrations mainly from lipids), ~1650 cm^{-1} (C═O stretching of the amide group in proteins), and ~788 cm^{-1} (nucleic acid vibrations).[32–34] In the glucose–glutamine condition (Fig. 4f), the strong bands at ~788, ~1000, and ~1440 cm^{-1} remain prominent, with additional features from nucleic acids (~670, ~950 cm^{-1}, O–P–O stretching) and proteins (~1050, ~1520 cm^{-1}, N–H bending/C–N stretching).[33,34] These extra variable peaks indicate a more complex metabolic response, consistent with glutamine's role as both a structural precursor and a major nitrogen donor supporting the synthesis of amino acids and nucleotides, including purines and pyrimidines, in the cytoplasm.[35]

Notably, the broad features observed in the diagonal plots, such as the ~1570–1650 cm^{-1} region in the glucose-only

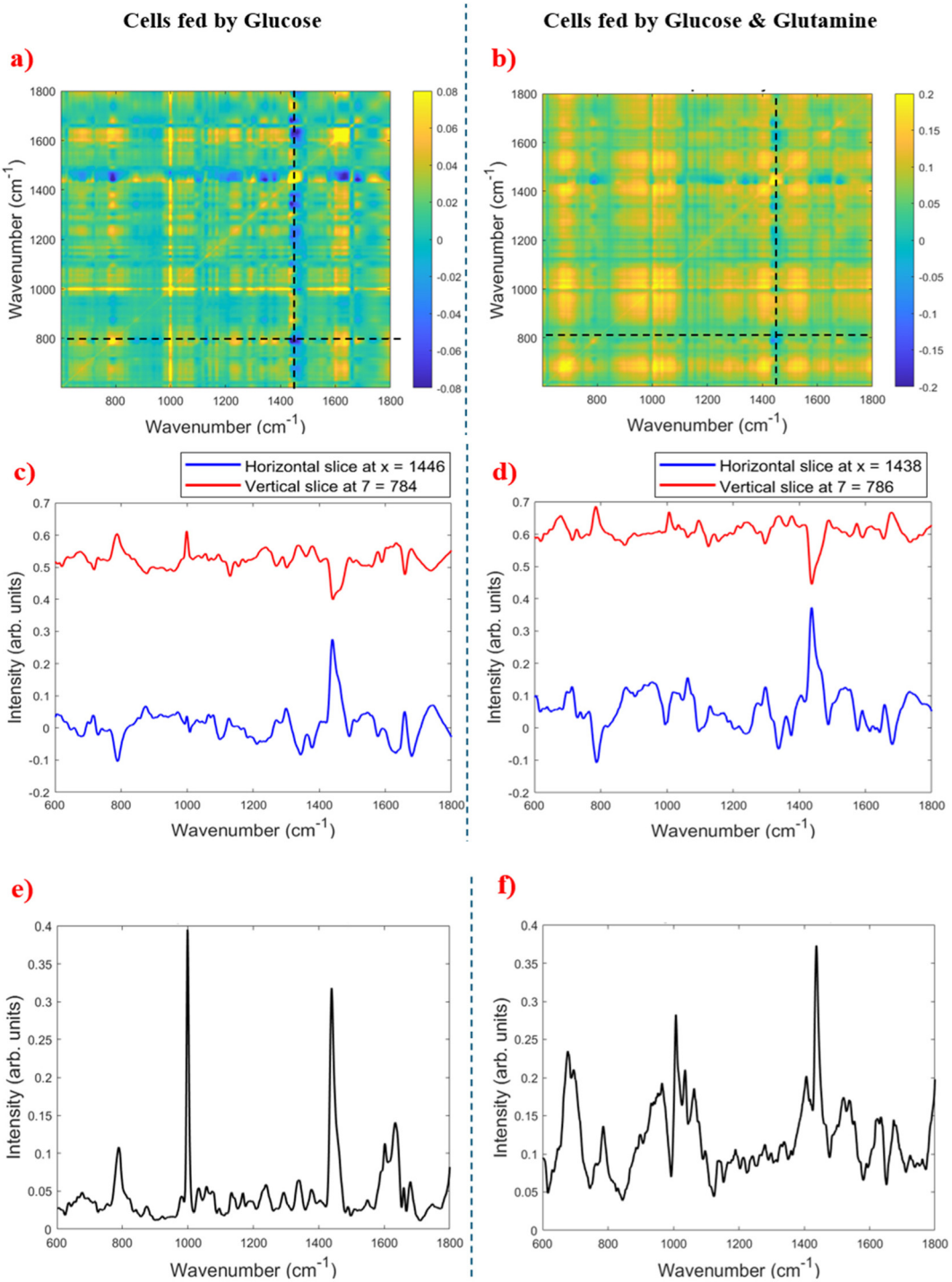

Fig. 4 2D correlation spectroscopy (2D-COS) results for cells fed with glucose (left panels) and glucose–glutamine (right panels). (a and b) Auto-synchronous 2D-COS maps highlighting correlated spectral changes across the 600–1800 cm^{-1} region. (c and d) Representative horizontal and vertical slices at selected wavenumbers, illustrating band-specific correlation behaviour. (e and f) Diagonal plots of the 2D-COS maps, identifying the most variable peaks in each condition.

sample, and several broad shoulders in the glucose–glutamine sample, including ~630–750, ~850–1000, and ~1050–1150 cm^{-1}, likely arise from the combined contributions of multiple biomolecules. When several overlapping vibrational modes vary on similar time scales, their signals merge into broad peaks rather than sharp, well-resolved bands. All peaks identified from the auto-synchronous diagonal plots were subsequently tracked as a function of time to compare the kinetic evolution of glucose-only and glucose–glutamine conditions. The corresponding plots, which include all

replicates at each time point as well as averaged trends for clearer visualisation, are shown in Fig. S7.

As presented in Fig. 5, many peaks display strong similarities in their temporal trajectories under both nutritional conditions. These coordinated trajectories occur across bands assigned to different biomolecular classes such as lipids, nucleic acids, proteins, and carbohydrates, as detailed in Table S1. Notably, in the glucose-only condition, the coordinated peaks exhibit an overall trend which seems to increase, decrease, and increase again, as a function of time. Such oscillations in band intensities may reflect intrinsic glycolytic oscillations, a well-documented phenomenon whereby metabolite concentrations fluctuate rhythmically due to inherent feedback regulation within glycolysis.[36] In 1967, Ibsen and Schiller reported oscillations of nucleotides and glycolytic intermediates in aerobic suspensions of starved Ehrlich ascites tumour cells following the addition of glucose.[37] More recently, glycolytic oscillations have also been observed in HeLa cervical cancer cells at the single-cell level using a monolayer culture system.[38] One likely reason why only a few studies have reported glycolytic oscillations in cells is the inherently low degree of synchronisation between individual cells, which makes such dynamics difficult to detect at the population level.[38] So, the patterns observed in this study could reflect partial synchronisation, potentially induced by the 2 h starvation step prior to nutrient exposure, which resets cellular metabolism and triggers a partially coordinated recovery response upon refeeding.

In the glucose–glutamine samples, the addition of glutamine resulted in smoother metabolic dynamics over the first hour, followed by more pronounced changes over the second hour compared with glucose alone. Interestingly, the maximum intensity of these coordinated peaks occurred about 15 minutes earlier in the glucose–glutamine condition (~90 min) than in the glucose-only condition (~105 min), and, unlike in the glucose-only sample, the overall trend continued to rise at the final time point of the experiment. These observations suggest that glutamine not only enhanced the variability of the metabolic response but also accelerated the overall cellular dynamics, consistent with its dual role in supporting biosynthetic and bioenergetic processes.[6]

In addition to examining intensity profiles, the differential 2D-COS evolution of two variable bands (788 and 1440 cm^{-1}) was evaluated for both samples (Fig. 6). In this approach, the synchronous diagonal element is recalculated for each successive interval (*e.g.*, 0–15, 15–30 min), highlighting periods when a band shows greater or lesser dynamic variance relative to the first interval. Unlike raw intensity plots that reflect absolute signal changes, this method pinpoints the specific intervals contributing most to kinetic fluctuations: peaks mark increased activity, while troughs indicate relative stability.

For the band at 788 cm^{-1} (Fig. 6a), mainly corresponding to DNA/RNA vibrations (O–P–O stretching), the glucose sample shows an early rise at 30–45 min, followed by a temporary decrease and a later increase at ~90–120 min. This pattern may reflect transient changes in nucleic acid metabolism, such as an early transcriptional response to glucose availability, characterised by rapid RNA synthesis and short-term metabolic reprogramming *via* energy-sensing pathways.[39–41] As an illustrative example, the Fos gene, a well-known gene to early transcriptional response, is rapidly induced after stimulation, peaking at 30–60 min and returning to basal levels by ~90 min.[42] In contrast, in the glucose–glutamine sample, this band exhibits a delayed activation (after ~60 min) compared to glucose alone. This shift might be associated with glutamine's multifaceted metabolic role, although contributions from other pathways cannot be excluded. Glutamine supplies nitrogen for purine and pyrimidine synthesis and, through glutami-

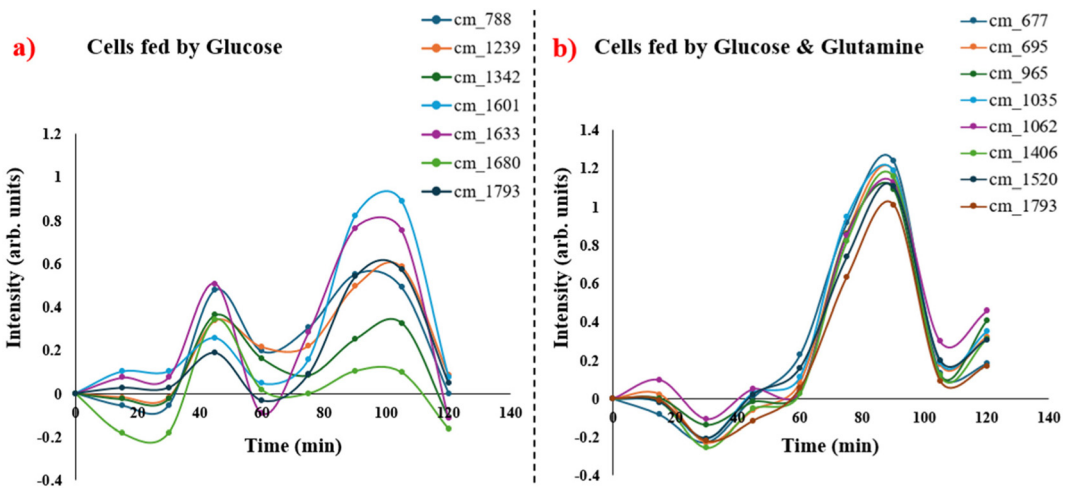

Fig. 5 Temporal evolution of selected Raman bands in cells fed with (a) glucose or (b) glucose–glutamine. Each time point represents 25 single-cell measurements (biological replicates), with no additional technical averaging applied. The plotted curves show the mean intensity profiles of the selected Raman bands over the 0–120 min period (15 min intervals), illustrating differences in intracellular dynamic responses between the two nutritional conditions.

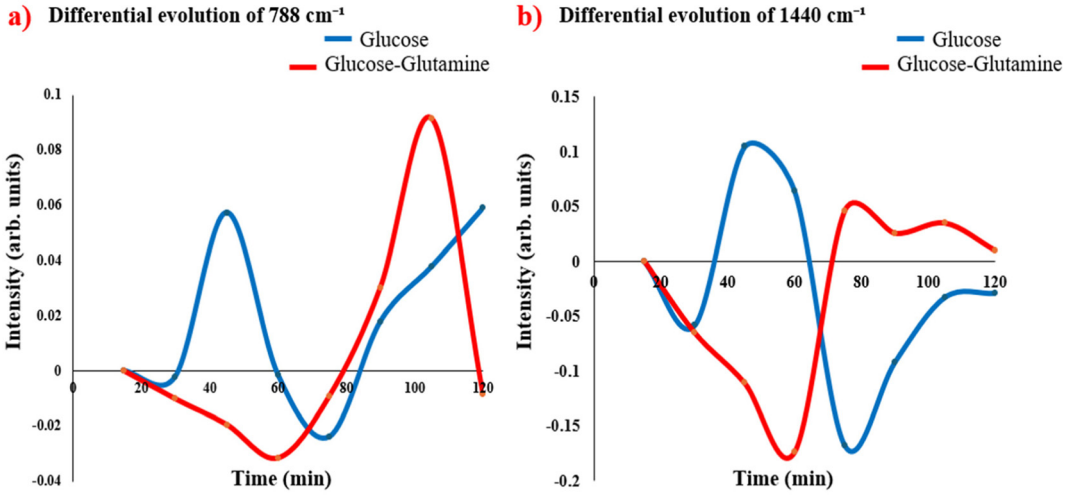

Fig. 6 Differential 2D-COS evolution of the nucleic acid band (788 cm^{-1}, panel a) and the lipid band (1440 cm^{-1}, panel b) in cells fed with glucose (blue) or a glucose–glutamine mixture (red).

nolysis, is converted to glutamate and subsequently α-ketoglutarate, replenishing the TCA cycle *via* anaplerosis.[6] By providing both nitrogen and TCA intermediates, glutamine may transiently reduce the reliance on glucose-derived carbon for nucleotide biosynthesis during the early phase of nutrient exposure. As glutamine metabolism becomes progressively engaged, nucleotide precursor pools are replenished more gradually, leading to a delayed but sustained increase in RNA-associated spectral signals.[43,44] It should also be recognised that glucose and glutamine participate in multiple interconnected metabolic pathways; therefore, some of the observed spectral variations may arise from parallel processes such as amino acid synthesis, redox regulation, and energy metabolism, rather than exclusively from the glycolysis–glutaminolysis axis.

Similarly, for the ~1440 cm^{-1} band (Fig. 6b), associated with lipid CH_2 vibrations, the glucose condition shows an early increase that might involve the same early response signals as the transcriptional activation. Cellular exposure to glucose can activate nutrient-responsive signalling pathways that stimulate anabolic processes, including protein and lipid biosynthesis. Consistent with this, the study by Porstmann *et al.*[45] demonstrated that glucose-responsive phosphoinositide 3-kinase/protein kinase B (PI3K/Akt) signalling promotes coordinated increases in protein and lipid synthesis by activating anabolic transcriptional programs, including sterol regulatory element-binding protein (SREBP)-regulated lipogenic pathways, which could contribute to the early increas in lipid-associated Raman signals observed here.

For the glucose–glutamine sample, the ~1440 cm^{-1} band, indicative of lipid-related fluctuations, emerges later (from ~75 min onward). This delay may be linked to glutamine's role in replenishing the TCA cycle, which gradually generates citrate that can be exported to the cytosol to support *de novo* fatty acid and lipid biosynthesis.[46]

4. Conclusion

This study demonstrated the potential of label-free Raman microspectroscopy, combined with 2D-COS, for mining complex time-resolved spectral datasets and resolving metabolic dynamics at the single-cell level. Simulated datasets first confirmed that 2D-COS can reliably distinguish variable peaks associated with glucose, RNA, lactate, and glutamine, allowing their kinetic behaviours to be tracked even under strong cellular background signals (up to weights of 40). These results highlight the sensitivity and reliability of 2D-COS for monitoring metabolic pathway kinetics in noisy conditions.

Experimental Raman spectra from cells exposed to two nutritional conditions (glucose alone or glucose plus glutamine) were then analysed using 2D-COS. Auto-synchronous maps (diagonal peaks) revealed coordinated temporal trajectories across multiple biomolecular bands, reflecting partially synchronised metabolic behaviour likely induced by the starvation step prior to nutrient exposure. Oscillatory patterns observed in glucose-only samples are consistent with intrinsic glycolytic oscillations, whereby metabolite levels fluctuate periodically due to feedback regulation within glycolysis. In contrast, glutamine supplementation smoothed early metabolic dynamics but produced more pronounced responses later, peak responses occurring earlier (~90 min *vs.* ~105 min) and continuing to rise. This suggests that glutamine accelerates and amplifies metabolic activity, consistent with its biosynthetic and bioenergetic roles.

Differential 2D-COS analysis of the 788 and 1440 cm^{-1} bands further highlighted distinct temporal coordination between nucleic acid and lipid dynamics. In glucose-only samples, both bands showed early activation, consistent with rapid transcriptional and lipid biosynthetic responses triggered by glucose re-feeding. In the glucose–glutamine condition, these bands displayed delayed but sustained activation,

reflecting glutamine's contribution to nucleotide biosynthesis and anaplerotic metabolism, which gradually supports RNA and lipid production.

Overall, while cells under both conditions shared common dynamic peaks, the glucose–glutamine samples exhibited stronger correlations and additional variable bands, particularly linked to nucleic acid vibrations, suggesting enhanced nucleotide biosynthesis. These findings indicate that glutamine not only accelerates and amplifies overall metabolic variability but also drives specific biosynthetic pathways, underscoring its broader role in cellular metabolism beyond energy provision. Beyond the specific metabolic findings, this work demonstrates how 2D-COS can complement existing chemometric approaches for analysing time-resolved single-cell Raman datasets. The ability of 2D-COS to reveal coherent temporal patterns offers a framework that can be extended to a wide range of applications, including drug-response profiling, metabolic stress testing, stem-cell differentiation, and bioprocess optimisation. These capabilities suggest that 2D-COS could enhance future single-cell studies and contribute to translational applications, including cancer research and treatment development.

To avoid misinterpretation, several points and limitations should be acknowledged. The simulated kinetics provide only an idealised representation of metabolic behaviour for assessing the performance of 2D-COS, as they were generated using simplified ODE-based models that do not capture nonlinear feedback, regulation, compartmentalisation, or enzyme saturation effects present in real cellular systems. Likewise, the use of fixed rate constants represents an approximation, given that reaction rates in living cells are variable and context-dependent. Furthermore, the experimental analysis was performed on a single cell line under two defined nutritional conditions, and only synchronous 2D-COS was explored. These factors constrain the generalisability of the findings, and future studies employing different cell lines, larger cell populations, and additional perturbations will be essential for further validating the findings and extending the analytical potential of 2D-COS. Moreover, direct measurement of glucose and glutamine uptake or depletion in the spent media, and correlating these changes with intracellular Raman dynamics, would provide a stronger metabolic context and represents a valuable direction for future work.

Author contributions

Zohreh Mirveis: conceptualisation, writing – original draft, Nitin Patil: conceptualisation, Hugh J. Byrne: conceptualisation, writing – review & editing, supervision, funding acquisition.

Conflicts of interest

There are no conflicts of interest to declare.

Data availability

The datasets supporting this article, including raw single-cell Raman spectra, and MATLAB scripts for preprocessing (PCA and EMSC correction), loading spectra for 2D-COS analysis, and reproducing key figures, are openly available on Zenodo at https://zenodo.org/records/17404836. The dataset also includes the data used for simulations (components and control cell spectra) with corresponding MATLAB code.

Supplementary information is available. See DOI: https://doi.org/10.1039/d5an01114k.

Acknowledgements

This work was supported by Research Ireland Frontiers for the Future Award [grant numbers: 20/FFPP/8517]. Open access funding provided by IReL.

References

1 R. I. K. Geltink, R. L. Kyle and E. L. Pearce, Unraveling the Complex Interplay between T Cell Metabolism and Function, *Annu. Rev. Immunol.*, 2018, **36**, 461–488.
2 P. Jasbi, A. E. Mohr, M. H. S. Murthy, *et al.*, Understanding metabolic resilience by unraveling temporal dynamics of cellular responses, *Trends Endocrinol. Metab.*, 2025, **36**(12), 1084–1098.
3 Z. Mirveis, N. Patil and H. J. Byrne, Experimental and computational investigation of the kinetic evolution of the glutaminolysis pathway and its interplay with the glycolysis pathway, *FEBS Open Bio*, 2024, **14**, 1247–1263.
4 N. Patil, Z. Mirveis and H. J. Byrne, Monitoring cellular glycolysis pathway kinetics in the extracellular medium using label-free, Raman spectroscopy, *Spectrochim. Acta, Part A*, 2025, **340**, 126363.
5 C. Li, G. Zhang, L. Zhao, *et al.*, Metabolic reprogramming in cancer cells: Glycolysis, glutaminolysis, and Bcl-2 proteins as novel therapeutic targets for cancer, *World J. Surg. Oncol.*, 2016, **14**, 1–7.
6 Z. Mirveis, O. Howe, P. Cahill, *et al.*, Monitoring and modelling the glutamine metabolic pathway: a review and future perspectives, *Metabolomics*, 2023, **19**(8), 1–24.
7 S. Siddhanta, A. N. Kuzmin, A. Pliss, *et al.*, Advances in Raman spectroscopy and imaging for biomedical research, *Adv. Opt. Photonics*, 2023, **15**(2), 318–384.
8 L. L. Lin, R. Alvarez-Puebla, L. M. Liz-Marzán, *et al.*, Surface-Enhanced Raman Spectroscopy for Biomedical Applications: Recent Advances and Future Challenges, *ACS Appl. Mater. Interfaces*, 2025, **17**, 16287–16379.
9 Y. Lu, L. Lin and J. Ye, Human metabolite detection by surface-enhanced Raman spectroscopy, *Mater. Today Bio*, 2022, **13**, 100205.

10 N. Kuhar, S. Sil, T. Verma, *et al.*, Challenges in application of Raman spectroscopy to biology and materials, *RSC Adv.*, 2018, **8**, 25888–25908.
11 D. Wang, P. He, Z. Wang, *et al.*, Advances in single cell Raman spectroscopy technologies for biological and environmental applications, *Curr. Opin. Biotechnol*, 2020, **64**, 218–229.
12 R. Gautam, S. Vanga, F. Ariese, *et al.*, Review of multidimensional data processing approaches for Raman and infrared spectroscopy, *EPJ Tech. Instrum.*, 2015, **2**(1), 1–38.
13 I. Noda, Two-Dimensional Correlation Spectroscopy (2D-COS) Analysis of Evolving Hyperspectral Images, *Appl. Spectrosc.*, 2025, **79**, 77–86.
14 H. G. Schulze, S. Rangan, M. Z. Vardaki, *et al.*, Two-Dimensional Clustering of Spectral Changes for the Interpretation of Raman Hyperspectra, *Appl. Spectrosc.*, 2022, **77**, 835.
15 J. Hniopek, T. Bocklitz, M. Schmitt, *et al.*, Probing Protein Secondary Structure Influence on Active Centers with Hetero Two-Dimensional Correlation (Resonance) Raman Spectroscopy: A Demonstration on Cytochrome C, *Appl. Spectrosc.*, 2021, **75**, 1043.
16 A. Kołodziej, M. Rachwał, M. Ziąbka, *et al.*, Two-dimensional correlation Raman spectroscopic study of the bioactivity of polycaprolactone-hydroxyapatite composites, *J. Mol. Struct.*, 2025, 143910.
17 P. Lasch and I. Noda, Two-Dimensional Correlation Spectroscopy (2D-COS) for Analysis of Spatially Resolved Vibrational Spectra, *Appl. Spectrosc.*, 2019, **73**, 359–379.
18 Z. K. Wang, N. Ta, H. C. Wei, *et al.*, Research of 2D-COS with metabolomics modifications through deep learning for traceability of wine, *Sci. Rep.*, 2024, **14**, 1–10.
19 H. J. Byrne, F. Bonnier and Z. Farhane, Two-dimensional correlation analysis of Raman microspectroscopy of subcellular interactions of drugs in vitro, *J. Biophotonics*, 2019, **12**, e201800328.
20 Z. Mirveis, N. Patil and H. J. Byrne, Exploring cellular metabolic kinetics through spectroscopic analysis of extracellular environments, *Spectrochim. Acta, Part A*, 2025, **340**, 126308.
21 N. Patil, Z. Mirveis and H. J. Byrne, Kinetic modelling of the cellular metabolic responses underpinning in vitro glycolysis assays, *FEBS Open Bio*, 2024, **14**, 466–486.
22 Vikstrom S and Technologies A pH xtra glycolysis assay user guide. https://www.agilent.com/cs/library/usermanuals/public/5991-9329EN_pH_Xtra_User_Guide.pdf.
23 L. T. Kerr and B. M. Hennelly, A multivariate statistical investigation of background subtraction algorithms for Raman spectra of cytology samples recorded on glass slides, *Chemom. Intell. Lab. Syst.*, 2016, **158**, 61–68.
24 I. Noda, Advances in two-dimensional correlation spectroscopy, *Vib. Spectrosc.*, 2004, **36**, 143–165.
25 I. Noda and Y. Ozaki, *Two-dimensional correlation spectroscopy: applications in vibrational and optical spectroscopy*, 2004, p. 295.
26 Mat2dcorr - A Matlab Toolbox for 2D-COS - 2D-COS Wiki, https://wiki2dcos.microbe-ms.com/index.php?title=Mat2dcorr_-_A_Matlab_Toolbox_for_2D-COS (accessed 25 September 2025).
27 L. C. Flores-García, V. García-Castillo, E. Pérez-Toledo, *et al.*, HOTAIR Participation in Glycolysis and Glutaminolysis Through Lactate and Glutamate Production in Colorectal Cancer, *Cells*, 2025, **14**, 388.
28 M. A. Medina, N. Ignacio and De Castro, Glutaminolysis and glycolysis interactions in proliferant cells, *Int. J. Biochem.*, 1990, **22**, 681–683.
29 C. Bergès, E. Cahoreau, P. Millard, *et al.*, Exploring the glucose fluxotype of the e. Coli y-ome using high-resolution fluxomics, *Metabolites*, 2021, **11**, 271.
30 K. E. Wellen and C. B. Thompson, Cellular Metabolic Stress: Considering How Cells Respond to Nutrient Excess, *Mol. Cell*, 2010, **40**, 323–332.
31 P. Thomas, G. Terradot, V. Danos, *et al.*, Sources, propagation and consequences of stochasticity in cellular growth, *Nat. Commun.*, 2018, **9**, 1–11.
32 Raman Spectroscopy and Applications.
33 C. Krafft, T. Knetschke, R. H. W. Funk, *et al.*, Studies on Stress-Induced Changes at the Subcellular Level by Raman Microspectroscopic Mapping, *Anal. Chem.*, 2006, **78**, 4424–4429.
34 I. Notingher, Raman Spectroscopy Cell-based Biosensors, *Sensors*, 2007, **7**, 1343–1358.
35 Y. Zhu, T. Li, S. R. Da Silva, *et al.*, A critical role of glutamine and asparagine γ-Nitrogen in nucleotide biosynthesis in cancer cells hijacked by an oncogenic virus, *mBio*, 2017, **8**(4), DOI: 10.1128/mbio.01179-17.
36 D. D. van Niekerk, M. van Wyk, T. Kouril, *et al.*, Kinetic modelling of glycolytic oscillations, *Essays Biochem.*, 2024, **68**, 15–25.
37 K. H. Ibsen and K. W. Schiller, Oscillations of nucleotides and glycolytic intermediates in aerobic suspensions of Ehrlich ascites tumor cells, *Biochim. Biophys. Acta, Bioenerg.*, 1967, **131**, 405–407.
38 T. Amemiya, K. Shibata and T. Yamaguchi, Metabolic Oscillations and Glycolytic Phenotypes of Cancer Cells, *Int. J. Mol. Sci.*, 2023, **24**, 11914.
39 D. A. Glauser, T. Brun, B. R. Gauthier, *et al.*, Transcriptional response of pancreatic beta cells to metabolic stimulation: Large scale identification of immediate-early and secondary response genes, *BMC Mol. Biol.*, 2007, **8**, 1–15.
40 H. X. Yuan, Y. Xiong and K. L. Guan, Nutrient Sensing, Metabolism, and Cell Growth Control, *Mol. Cell*, 2013, **49**, 379–387.
41 S. Aitken, S. Magi, A. M. N. Alhendi, *et al.*, Transcriptional Dynamics Reveal Critical Roles for Non-coding RNAs in the Immediate-Early Response, *PLoS Comput. Biol.*, 2015, **11**, e1004217.
42 S. Bahrami and F. Drabløs, Gene regulation in the immediate-early response process, *Adv. Biol. Regul.*, 2016, **62**, 37–49.
43 J. P. Mazat and S. Ransac, The Fate of Glutamine in Human Metabolism. The Interplay with Glucose in Proliferating Cells, *Metabolites*, 2019, **9**, 81.
44 R. J. Deberardinis and T. Cheng, Q's next: The diverse functions of glutamine in metabolism, cell biology and cancer, *Oncogene*, 2010, **29**, 313–324.

45 T. Porstmann, C. R. Santos, B. Griffiths, *et al.*, SREBP Activity Is Regulated by mTORC1 and Contributes to Akt-Dependent Cell Growth, *Cell Metab.*, 2008, **8**, 224–236.

46 I. J. Muyinda, J. G. Park, E. J. Jang, *et al.*, KRAS, A Prime Mediator in Pancreatic Lipid Synthesis through Extra Mitochondrial Glutamine and Citrate Metabolism, *Int. J. Mol. Sci.*, 2021, **22**, 5070.